



Multiple-ScS probing of the Ontong-Java Plateau

B.M. Gomer*, E.A. Okal

Department of Geological Sciences, Northwestern University, Evanston, IL 60208, USA

Received 19 August 2002; accepted 22 April 2003

Abstract

We use multiple-ScS phases recorded at Pohnpei from a 1996 deep earthquake under the Solomon Islands to investigate the shear velocity and attenuation characteristics of the upper mantle under the Ontong-Java Plateau in the Western Equatorial Pacific. Cross-correlation results indicate a vertical one-way travel-time under the plateau 3 s slow with respect to PREM, in agreement with previously obtained tomographic results, which revealed the existence of an anomalously slow root under the plateau. Additionally, the study of stacked spectral ratios suggests an unusually high $Q_{\text{ScS}} = 366$, with a lower limit of $Q_{\text{ScS}} \geq 253$. This value is considerably higher than elsewhere in the Pacific, suggesting the absence of an asthenospheric layer under the edifice. The combination of slow shear-wave speed and lower than average shear attenuation rules out a temperature anomaly as the source of the Ontong-Java Plateau (OJP) root, which must then be related to a chemical or mineralogical heterogeneity. © 2003 Elsevier B.V. All rights reserved.

Keywords: Multiple-ScS; Asthenospheric layer; Large igneous province

1. Introduction

We present the results of the analysis of multiple-ScS phases to assess the properties of the mantle beneath the Ontong-Java Plateau (OJP). The OJP is an L-shaped, large igneous province (LIP) located in the westcentral Pacific between the Solomon Islands to the south and the Caroline Islands to the north (Fig. 1). Covering an area of roughly $1.6 \times 10^6 \text{ km}^2$, with an average elevation of 2000 m above the surrounding basin floor, the OJP is the largest LIP on Earth.

In a recent passive seismic experiment using four stations deployed in the Caroline Islands and Nauru, Richardson et al. (2000; hereafter Paper I) used Rayleigh wave partitioned waveform inversion (PWI) to obtain a tomographic image of the crust and up-

per mantle structure below the OJP. They found an average crustal thickness of 33 km with a maximum thickness of 38 km in the southcentral portion of the plateau. Comparable values of crustal thickness have been reported for other oceanic structures believed to have formed near mid-ocean ridges, including the Tuamotu Plateau (25–32 km; Talandier and Okal, 1987), the Iceland-Færøe Ridge (25–30 km; Bott and Gunnarsson, 1980), and the Nazca Ridge (18 km; Woods and Okal, 1994). However, the most intriguing result from Paper I was the presence of a low-velocity root extending as deep as 300 km beneath the OJP, over a lateral dimension of 600 km, and featuring mantle shear-wave speeds deficient by as much as 5% with respect to PREM (Dziewonski and Anderson, 1981), i.e. reaching below 4 km/s in places. Additional evidence for the OJP root was obtained from the interpretation of shear-wave splitting due to upper mantle anisotropy at the four temporary stations of the passive experiment, the fast polarization directions

* Corresponding author. Tel.: +1-847-491-5379;

fax: +1-847-491-8060.

E-mail address: bgomer@earth.northwestern.edu (B.M. Gomer).

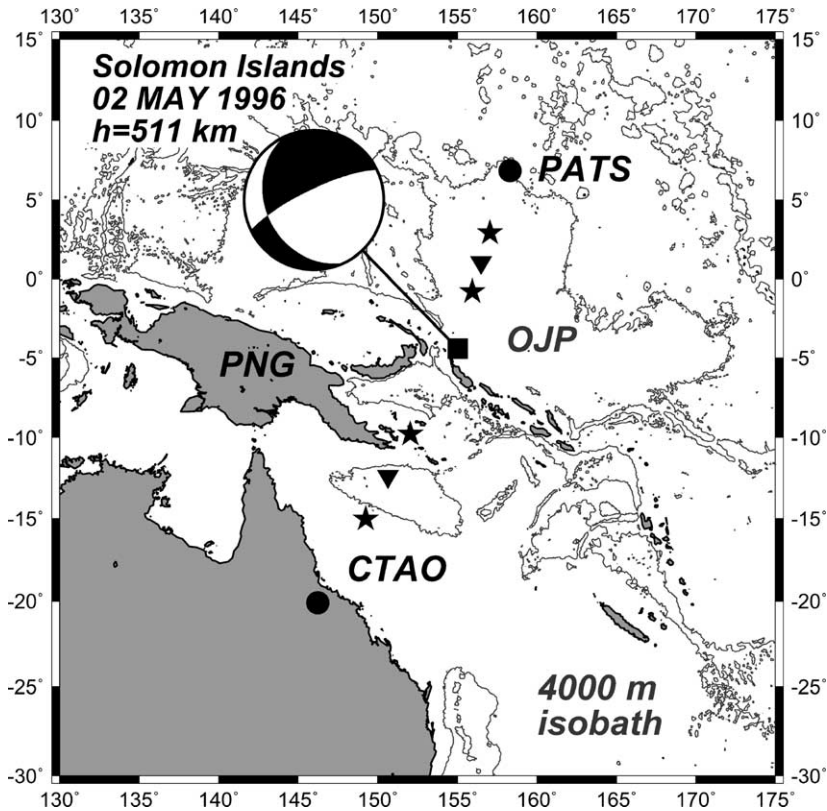


Fig. 1. Map of the study area, including the Ontong-Java Plateau, outlined East of Papua New Guinea (PNG) by the 4000 m isobath, the only one contoured on this plot. The epicenter (square) and focal mechanism of the source event are shown. Station PATS (solid circle), located along the northern edge of the OJP recorded multiple-ScS phases with bounce points under the plateau, shown as an inverted triangle (ScS₂) and stars (ScS₃). The reference path to station CTAO is shown similarly.

displaying a pattern of mantle flow detouring around the OJP. The plateau, thus, constitutes an obstacle to mantle flow in the form of a keel beneath the OJP (Klosko et al., 2001).

Such low-velocity structures at comparable depths have been previously reported only in areas involving active spreading centers such as the Kolbeinsey Ridge north of Iceland (Evans and Sacks, 1979), and are generally associated with substantial thermal anomalies. However, as compiled in Paper I, a thermal origin for the OJP low-velocity root is unlikely on the basis of the 25 available heat flow measurements ranging from 0.4 to 1.9 HFU (17–80 mW/m²), with an average value of 1.1 HFU (47 mW/m²). These values do not indicate the presence of a heat flow anomaly and are actually lower than the average heat flow values in the nearby Nauru Basin (1.25 HFU or 52 mW/m²),

which include two to four times as many large heat flow values (i.e. >70 mW/m²). Furthermore, radiometric dating of OJP volcanic samples dates the main eruption at 121 ± 1 Ma, with a final burst of activity at 92 ± 2 Ma in the eastern part of the province (Mahoney et al., 1993). The long time elapsed since the emplacement of the LIP would allow significant cooling, and no possibility of detecting a thermally produced seismic velocity anomaly related to OJP formation (Woods and Okal, 1996; Yoshida and Suetsugu, 2000). If the observed deficit in shear-wave velocity is not thermal in origin, then some form of mineralogical or chemical anomaly is the likely source of velocity perturbation.

Seismic attenuation can be a further discriminant between a thermal or compositional nature for the OJP heterogeneity. Shear-wave attenuation, Q_{μ}^{-1} ,

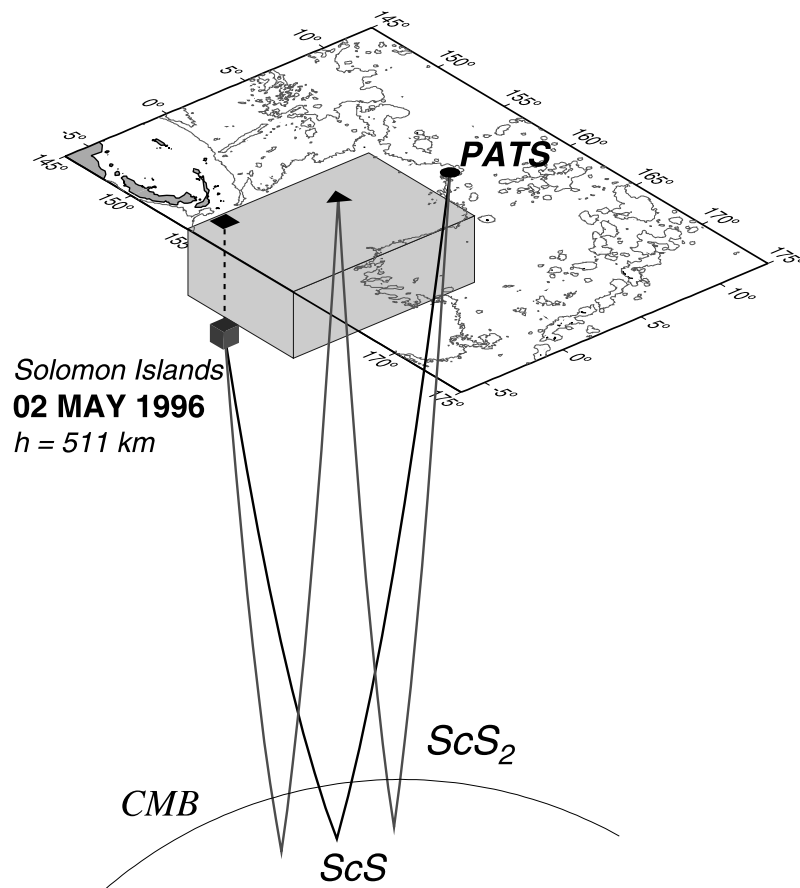


Fig. 2. Perspective sketch showing the Solomon Island epicenter (square), hypocenter (cube), receiving station (circle), and paths of ScS and ScS₂ reflecting on the core–mantle boundary (CMB). The shaded box sketches the location and extent of the OJP root, as determined by the inversion in Paper I, showing that reflected phases clearly sample the root.

is known to be strongly affected by temperature (Anderson, 1989), whereas a mineralogical or compositional variation may decrease the seismic wave speed, but preserve a high quality factor Q .

This paper explores the proposed OJP root using multiple-ScS phases with surface bounce points in the plateau. The general layout of our experiment is shown in Fig. 2, with the mid-path reflection of ScS₂ clearly sampling the proposed OJP root. This now classical technique (Okal and Anderson, 1975; Sipkin and Jordan, 1976, 1980; Suetsugu, 2000) provides a mechanism for probing the upper mantle beneath uninstrumented regions without the complications of near-source and near-receiver structures found in other types of body-wave studies. It allows both

an independent comparison of travel-time delays of multiple-ScS phases with the results of surface-wave tomography, and an opportunity to measure Q_{ScS} beneath the OJP using the spectral-ratio method.

2. Dataset

Multiple-ScS probing was not used in Paper I due to the lack of adequate earthquakes during the passive experiment. However, shortly after its conclusion, a deep earthquake (511 km) occurred on 2 May 1996 in the Solomon subduction zone, with a focal mechanism ($\phi = 250^\circ$, $\delta = 73^\circ$, $\lambda = -111^\circ$; Dziewonski et al. (1997)) favoring the generation of ScS waves. We use

the records from the permanent POSEIDON station at Pohnpei (PATS) to analyze the seismic properties of material beneath the OJP using ScS phase delay times and Q . We also use records at CTAO (Charter Towers, Australia) from the same Solomon Island event as a standard of comparison with a path that does not intersect the OJP root. This dataset, consisting of records of a single earthquake along a single path sampling the OJP structure, is limited. However, the results confirm slow seismic velocities within the OJP root and strongly indicate unusually low attenuation.

Fig. 3 shows broadband records at PATS ($\Delta = 11.7^\circ$) and CTAO ($\Delta = 17.8^\circ$). The time series (a and c) are band-passed with corners at 0.01 and 0.0625 Hz to clearly show the various ScS phases and the associated noise. Although the signal-to-noise ratio in this frequency band is not exceptionally high, a signal is clearly present in the time domain. For comparison, we plot the PATS time series (b) filtered with corners at 0.01 and 0.1 Hz. Noise obviously contaminates the signal above 0.0625 Hz making the identification of ScS₂ and ScS₃ difficult.

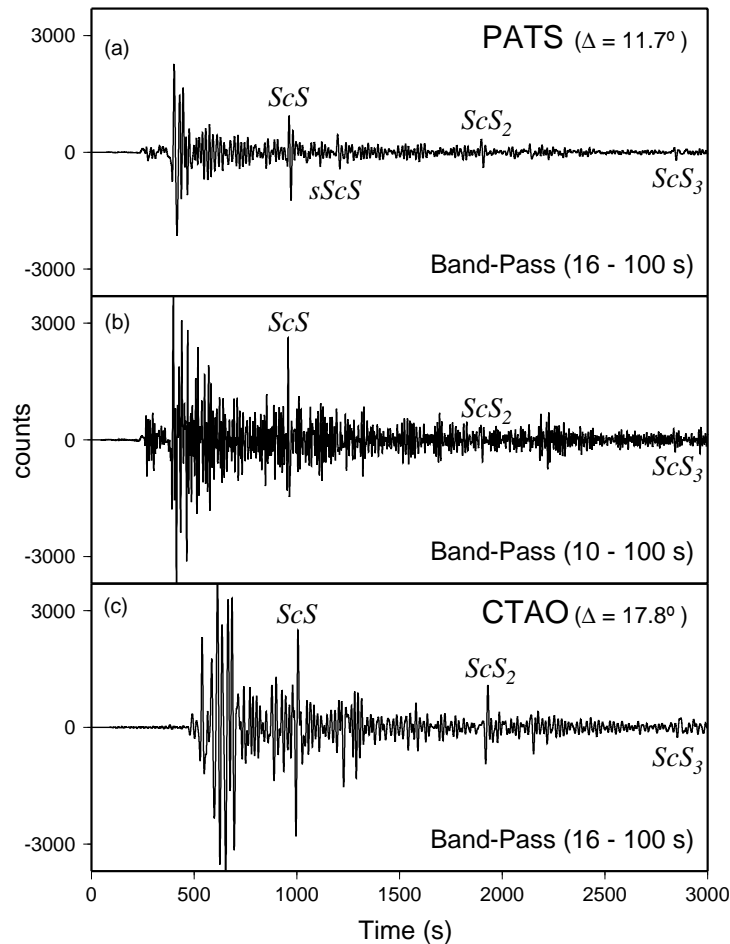


Fig. 3. Band-passed (16–100 s) broadband seismograms used in this study, at PATS (top) and the reference station CTAO (bottom). For each station, we show the transverse component and label the ScS_{*n*} ($n \leq 3$) and sScS₁ phases. The middle plot shows the band-passed (10–100 s) broadband seismogram at PATS for comparison with the upper plot. Note the ScS₂ and ScS₃ phases are obscured by noise above the 16 s cut-off used in the upper, more narrowly filtered PATS time series.

3. Travel-time residuals

3.1. Methodology

Our method is similar to those employed by earlier authors using ScS travel-time residuals in larger-scale studies of upper mantle heterogeneities (Okal and Anderson, 1975; Sipkin and Jordan, 1976). Differential travel-times ($\Delta t_{n,p}$) are computed by cross-correlating a set of two phases, ScS_n and ScS_p. These results are then compared to values measured by the same cross-correlation algorithm applied to synthetic seismograms computed using the PREM model (Dziewonski and Anderson, 1981) with an el-

lipticity correction (Dziewonski and Gilbert, 1976), the Harvard CMT solution for the 1996 Solomon event, and the reflectivity method. We define a differential residual $R_{n,p} = \Delta t_{n,p}^{\text{obs}} - \Delta t_{n,p}^{\text{comp}}$. Note that this value is a $2(n - p)$ -way residual, resulting from sampling the anomalous region twice for each surface reflection. This procedure minimizes the contribution of near-source and near-receiver velocity heterogeneities and assumes that any difference between the observed and calculated times is the result of lateral heterogeneities in the upper mantle near the surface bounce point[s], and not the product of the supposedly more homogeneous lower mantle.

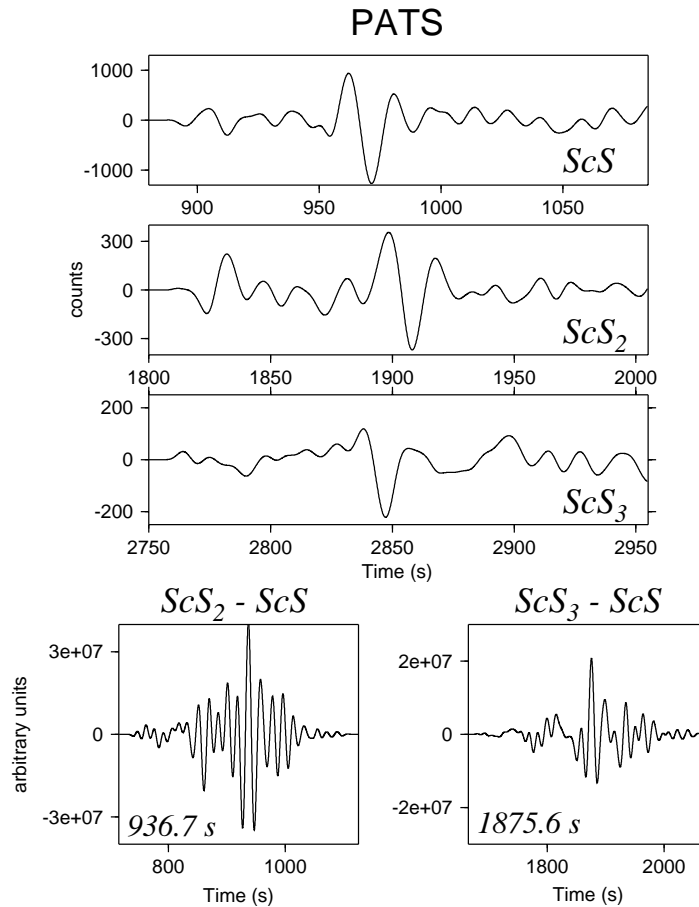


Fig. 4. Determination of differential travel-times $\Delta t_{2,1}$ and $\Delta t_{3,1}$ at PATS. Top: Band-passed records of the phases ScS, ScS₂ and ScS₃. Bottom: cross-correlation of the waveforms, with maxima at 936.7 and 1875.6 s. PREM synthetics in the same geometry yield values of 930.7 and 1865.6 s, respectively, resulting in a one-way travel-time residual in the root of 3 s.

3.2. Results at PATS

Cross-correlation measurements on records of ScS_2 and ScS , taken on the transverse component at PATS, produced a differential travel-time $\Delta t_{2,1}^{\text{obs}} = 936.7$ s (Fig. 4). PREM synthetics for the same geometry and focal mechanism had $\Delta t_{2,1}^{\text{comp}} = 930.7$ s. Thus, the residual between the ScS and ScS_2 phases is $R_{2,1} = 6.0$ s, or 3.0 s for a one-way path through the OJP root. We also compare measurements taken on the SV and SH components, the results (936.2 and 936.7 s, respectively) being essentially robust at a precision better than 0.3 s for the one-way residual (the sampling of the time series being 0.1 s at PATS). This amounts to saying that we could not identify any contribution to travel-time residuals induced by azimuthal anisotropy along the (mostly vertical) path of the central branch of ScS_2 un-

der the OJP, and this suggests that the OJP structure, including any root, is azimuthally isotropic. This important result supports Klosko et al.'s (2001) interpretation of observed azimuthal anisotropy of 1 s or more at stations bordering the structure (including PNI, also located on Pohnpei, only 19 km from PATS), as induced by asthenospheric mantle flow *outside* the OJP.

Similar measurements between ScS and ScS_3 , also shown in Fig. 4, yield $\Delta t_{3,1}^{\text{obs}} = 1875.6$ s, while synthetics feature $\Delta t_{3,1}^{\text{comp}} = 1865.6$ s, the differential residual thus being $R_{3,1} = 10.0$ s, or 2.5 s for a one-way path.

3.3. Reference values at CTAO

Similar analysis at CTAO yields cross-correlation measurements of $\Delta t_{2,1}^{\text{obs}} = 923.2$ s (Fig. 5) with synthetic calculations of 922.8 s for the same geometry.

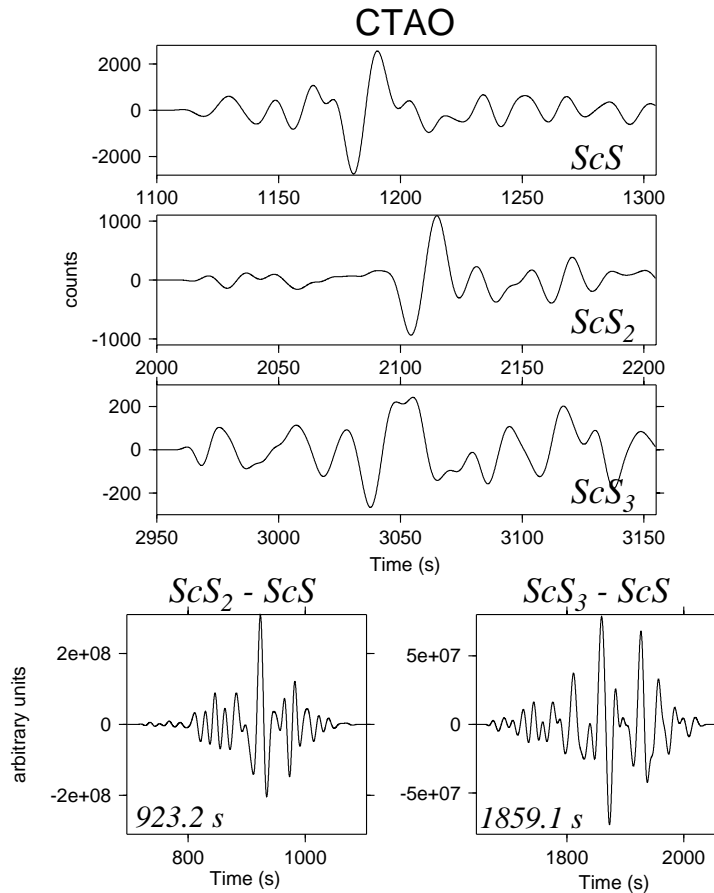


Fig. 5. Same as Fig. 4 for the reference station CTAO.

Therefore, the two-way $R_{2,1}$ value at CTAO is 0.4 s, or 0.2 s for a one-way path through the upper mantle. A value of 1859.1 s is obtained for $\Delta t_{3,1}^{\text{obs}}$, while the computed value for synthetic seismograms is 1855.0 s, which gives a four-way residual at CTAO $R_{3,1} = 4.1$ s, or 1 s for a one-way path. This reference dataset indicates the one-way travel path through the upper mantle beneath the Coral Sea is slow by 1 s, appreciably less than under the OJP root.

4. Measurement of Q

4.1. Methodology

Following the general method of Yoshida and Tsujiura (1975) and Sipkin and Jordan (1980), we use the spectral ratio between two phases, ScS_n and ScS_p , to evaluate Q_{ScS} . Specifically, we plot on Figs. 6a–c and 7a–c the spectral amplitudes $X(\omega)$ of the three phases, along with the background noise spectra (as determined from a window preceding the arrival of interest on the same component as the phases under study). This plot allows the visual assessment of a frequency range with appropriate signal-to-noise ratios. The ratio of the spectral amplitudes of any two phases is then best-fit by a straight line of the type $\ln(X_n(\omega)/X_p(\omega)) = -a\omega + b$, and Q_{ScS} simply retrieved from $Q_{\text{ScS}} = \Delta t_{n,p}/2a$. The derivation of this relationship is well established (e.g. Kovach and Anderson, 1964; Kanamori, 1967). In particular, the method has the advantage of eliminating any geometrical effects on the amplitude of a multiple-ScS phase, since the latter are expected to be frequency independent.

Our only modification to this method is in the estimation of the spectra. We use the multiple-taper method (MTM) (Thomson, 1982) to decrease the variance in our spectral estimate without arbitrarily smoothing a single-taper spectrum. Given a time series of N samples, x_n ($n = 1, 2, \dots, N$), the MTM uses a set of K orthonormal tapers ($h_{n,k}$), chosen to exhibit a specific property and computes K uncorrelated spectra. Averaging the K spectra produces a MTM spectral estimate (S_{MTM}).

$$S_{\text{MTM}}(\omega) = \frac{1}{K} \sum_{k=1}^K \sum_{n=1}^N \left| h_{n,k} x_n e^{-i\omega n \delta t} \right|^2 \quad (1)$$

A variety of weighted averages have been proposed for MTM estimates, but we choose a uniform weight. Multiple-taper methods are common in spectral studies of seismic waves (e.g. Lees and Lindley, 1994; Bhattacharyya et al., 1996). However, unlike these authors, we do not use the commonly cited Slepian tapers (also called Discrete Prolate Spheroidal Sequences (Slepian, 1978)). Instead, we use the sinusoidal tapers of Riedel and Sidorenko (1995).

$$h_{n,k} = \sqrt{\frac{2}{N+1}} \sin\left(\frac{\pi kn}{N+1}\right) \quad (2)$$

to compute K orthonormal tapers that minimize the spectral-window bias. A similar attempt at minimizing spectral-window bias led to Papoulis' (1973) optimal taper, which the first sine taper approximates.

Sinusoidal tapers allow a simple trade-off between resolution and variance without an additional bandwidth parameter (adding or deleting a sine taper increases or decreases the band width) or varying the amount of leakage protection. In contrast, Slepian tapers have predefined bandwidths and a variable amount of leakage protection depending on the number of tapers used in the spectral estimate. However, the simplicity of sine tapers comes at the price of moderate leakage protection compared to the lowest order Slepian tapers. This is not surprising since Slepian tapers maximize the concentration of spectral energy within a predefined bandwidth, and near the edge of the Slepian tapers' bandwidth they outperform sine tapers. Away from the Slepian bandwidth frequency, towards more central and more distant frequencies, sinusoidal tapers outperform Slepian tapers (Riedel and Sidorenko, 1995).

Spectral ratios for pairs of ScS phases are computed with the MTM spectra described above. MTM spectra also allow an internal, non-parametric measure of the spectral-ratio variance using the *jackknife* (Efron, 1982; Thomson and Chave, 1991). The delete-one jackknife computes the variance of the MTM spectral-ratio estimate by successively deleting each taper's ratio and averaging the remaining $K - 1$ ratios to form K delete-one spectral ratios. A variance estimate is found using the standard formula $\sigma^2 = (n - 1)/n \sum_{i=1}^K (S_i - S_{\text{MTM}})^2$ where S_i is the delete-one spectral ratio (with the i -th taper's ratio removed) and the term $((n - 1)/n)$ expresses the different sample sizes. We plot the jackknifed standard

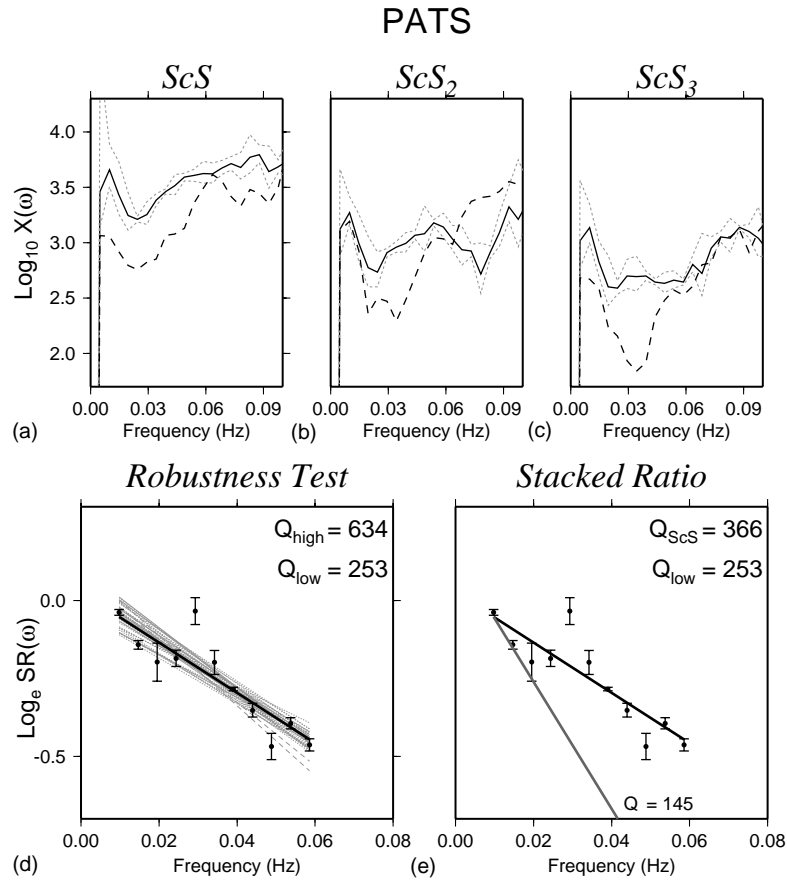


Fig. 6. Determination of Q_{ScS} at PATS, using the spectral ratios of ScS, ScS₂ and ScS₃. Top: Spectral amplitudes of the windowed traces of ScS (a), ScS₂ (b), and ScS₃ (c). Comparison with the preceding noise spectrum helps define an adequate frequency window. The light-grey dashed lines show the 1σ confidence interval of the spectral estimate. Although the noise spectrum intrudes into the confidence intervals, the time domain expression of the spectrum (Fig. 3) gives us confidence in the signal. (d) Robustness test for the stacked spectral estimate, $SR(\omega)$, at PATS. The thick dark line gives the slope of the best-fitting linear regression and the thin vertical lines show the jackknifed variance estimates. The grey lines depict 100 of the 2000 lines produced by randomly drawing normal deviates at each frequency and regressing unweighted lines. These lines produce a range of Q_{ScS} values that determine $Q_{high} = 634$ and $Q_{low} = 253$. (e) Stacked spectral-ratio estimate at PATS as a function of frequency. The thick dark line gives the slope of the best-fitting linear regression (same as d), from which Q_{ScS} is derived. The thin vertical lines show the standard deviation at each frequency determined by jackknifing. The half-toned segment labeled $Q = 145$ defines the upper bound of values which could be expected under the assumption of a thermal interpretation of the velocity anomaly.

deviation for the spectral ratios in Figs. 6, and 7e and f as vertical bars for reference. Estimates of the jackknifed standard deviation for individual spectra are also obtained using the individual spectral estimates from each taper. We plot the standard deviation as light-grey, dashed lines in Figs. 6, and 7a–c.

Jackknifed variance estimates for the spectral ratios are used as weights at each frequency during the linear

regression to determine Q_{ScS} . Then, to test the range of values expected from our Q_{ScS} estimates, we simulate 2000 Q_{ScS} values by randomly drawing normal deviates at each frequency with the standard deviation of the distribution determined by the jackknifed variance estimates (Bhattacharyya et al., 1996). For each set of random points, we regress an unweighted line and recompute Q_{ScS} . Since the jackknife tends to

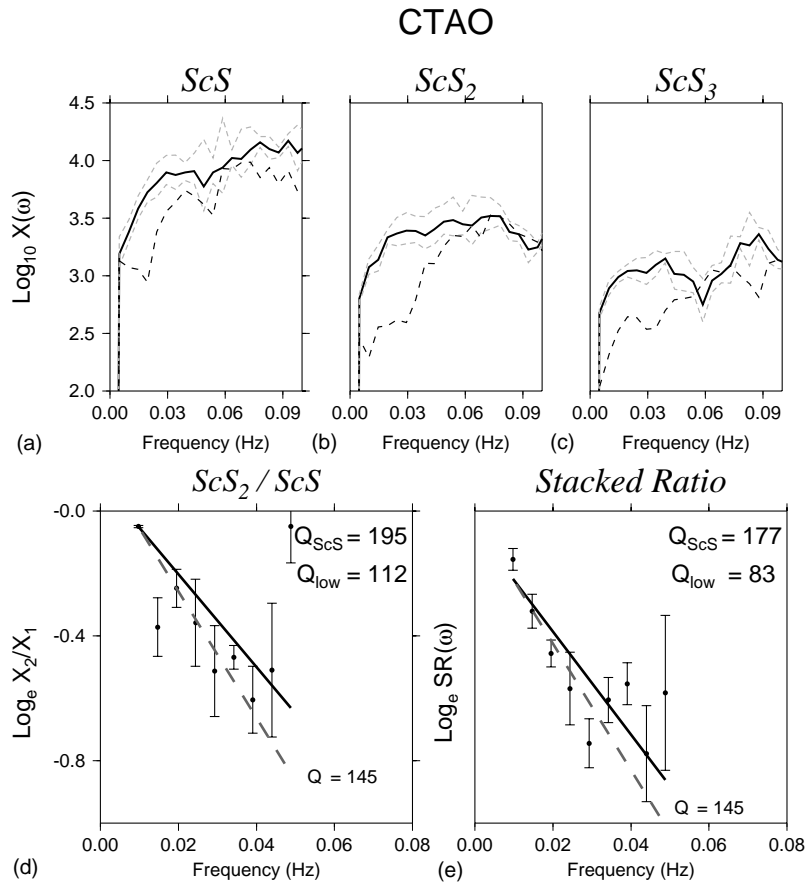


Fig. 7. Same as Fig. 6 for the reference station CTAO. However, (d) now depicts the ratio of ScS_2/ScS_1 , another statistically significant estimate of Q_{ScS} at CTAO. The notation follows those of the plot (e) at PATS.

overestimate the *true* variance, this test should provide a conservative estimate of the variability in Q_{ScS} values. We refer to the largest and smallest values produced by the simulation as Q_{high} and Q_{low} .

4.2. Results at PATS

Fig. 6a–c shows the spectral amplitudes for a 204.8 s long window for the transverse components of ScS , ScS_2 and ScS_3 at PATS, and compares them with background noise windowed immediately before the phase of interest. We also plot the jackknifed standard deviation to help determine an appropriate signal-to-noise ratio. Although the noise intrudes into the confidence intervals, we use frequencies from 0.1 to 0.0625 Hz.

This range is supported by our observations in the time domain, and is similar to typical windows used in other studies (Sipkin and Jordan, 1980). When attenuation is measured between 0.1 and 0.0625 Hz for the individual phase pairs, the best-fitting values are not statistically significant in a χ^2 sense (a linear relationship is not justified between frequency and the amplitude ratio). For the ScS_2/ScS_1 ratio the measured Q_{ScS} value is 755 with a $Q_{low} = 336$, while the ScS_3/ScS_1 and ScS_3/ScS_2 ratios produce Q_{ScS} values of 290 and 150, respectively, with Q_{low} of 227 and 106.

To overcome this problem, we correct for geometrical spreading and stack the spectra. This does not significantly reduce our spatial resolution since

the source–receiver distance is small and the surface reflection points lie in the OJP. Thus, the stacked value represents Q_{ScS} within the OJP and not the surrounding upper mantle structure. The best-fit value for our stacked spectrum is $Q_{\text{ScS}} = 366$, with $Q_{\text{low}} = 253$ and $Q_{\text{high}} = 634$. This line is statistically significant, but the goodness-of-fit is reduced due to overly conservative error estimates.

We will henceforth quote the value $Q_{\text{ScS}} = 366$, a statistically significant stacked value, but bear in mind the scatter in our robustness test. To a large extent, this scatter was expected, given the notoriously difficult measurements of any high value of an attenuation factor Q . More significant in our opinion than the value of the best-fitting Q_{ScS} is the high value of the lower bound, $Q_{\text{low}} = 253$. As discussed in more detail above, the robustness tests can be interpreted as failing to produce values of Q_{ScS} equal to or less than their global average.

We note here that Revenaugh and Jordan (1989) have cautioned against a possible bias on Q_{ScS} introduced by multiple reverberations inside the crustal layer; however, this effect becomes particularly significant on multiple ScS_n wave trains ($n > 3$), and should be minimal in our measurements. In addition, their Fig. 8 would suggest that Q_{S} could be biased upwards a maximum of 20%; it is unlikely that it would result in the higher measured value of Q_{ScS} as required by our conservative test for robustness described above.

The bottom line is that the OJP root features anomalously low anelastic attenuation for oceanic material of this age.

4.3. Results at CTAO

By contrast, we obtain a much lower stacked value, $Q_{\text{ScS}} = 177$, for the paths to CTAO, which reverberate under the Coral Sea. As shown on Fig. 7, the frequency band available for processing is narrower (20–100 s), and the lower and upper bounds range from 83 to infinity. An infinite Q_{high} is not surprising given the large variance associated with the higher-frequency end points. Again, this line is statistically significant, but the measurement of the $\text{ScS}_2/\text{ScS}_1$ phase pair also produced a meaningful value for $Q_{\text{ScS}} = 195$ with $Q_{\text{low}} = 112$. Thus, two measurements indicate Q_{ScS} values in the 175–200 range with a $Q_{\text{low}} \approx 100$.

5. Discussion and conclusion

5.1. Comparison with published values in neighboring provinces: travel times

Based on our measurement of $R_{2,1}$ at PATS, we document a one-way travel-time delay for shear waves (with respect to PREM) of 3.0 s for a ray reverberating in the central part of the OJP, near 1.08°N; 156.48°E. Our results using $R_{3,1}$ are slightly less slow, at 2.5 s (one-way). These one-way travel-time residuals are significantly greater than observed in the neighboring western Pacific basin or under oceanic lithosphere of an age comparable to the OJP basalts (−2.6 to +1.8 s) (Okal and Anderson, 1975; Sipkin and Jordan, 1976). The OJP mantle is also found slower than the tectonically complex area to the south along the path to CTAO.

In order to interpret our measurements in the framework of Paper I, we used the full three-dimensional model inverted by the PWI model and computed the vertical S travel-time delay which it predicts, relative to PREM, under the precise points of reverberation. This procedure, which includes the effects of both mantle heterogeneity and deflection of the crust, yields a one-way residual of 3.5 s at the bounce point of ScS_2 , and values of 3.4 and 3.7 s for the two bounce points of ScS_3 . These figures are somewhat lower than the simple model of a 5% deficiency extending to a depth of 300 km, on account of the irregularity of the inverted three-dimensional structure.

Our residual of 3.0 s is in generally good agreement with the model inverted in Paper I. It is clear, in particular, that a residual of this magnitude cannot be attributed exclusively to crustal deflection, since it would require a crustal thicknesses of at least 70 km. In this respect, our study brings an independent confirmation to the tomographic results of Paper I, namely that the OJP is underlain by a large root of anomalously slow material. In the case of the $R_{3,1}$ residual, our observed value (2.5 s) is slightly deficient with respect to the predictions of Paper I.

Finally, and for reference, the residuals at CTAO are well explained in the framework of Okal and Anderson's (1975) study: a two-way $R_{2,1}$ delay of 0.4 s for a bounce point under the Paleocene Coral Sea Basin, and a slower four-way $R_{3,1}$ delay of

4.1 s, involving bounce points under the active (and presumably slower) Woodlark Ridge.

5.2. Comparison with published values in neighboring provinces: Q_{ScS}

The Q value measured under the OJP, $Q_{ScS} = 366$ and more significantly, the lower bound on its error bar, $Q_{low} = 253$, are considerably higher than Q_{ScS} values reported by Sipkin and Jordan (1980) for the western Pacific basin ($Q_{ScS} = 155 \pm 11$, outside all our robustness tests). Note that the small error bars proposed by these authors reflect their use of stacking data relative to several earthquakes and distributed surface-reflection points. Similarly, Revenaugh and Jordan (1991) have proposed $Q_{ScS} = 169 \pm 30$ from Fiji to Hawaii, a path sampling slightly younger lithosphere. Our values are generally greater than those given by these authors ($Q_{ScS} = 226 \pm 30$) for a group of paths from New Britain to Taiwan, wholly west of the OJP. Our lowest Q_{low} value (253) does overlap with their error limits, but is likely overestimated. Their slightly higher value could also reflect interference of at least some reverberations within the subduction system at the Mariana corner. On the other hand, it is interesting to note Sipkin and Jordan's (1980) results along their so-called Fiji-MAT (Matsushiro, Japan) paths ($Q_{ScS} = 176 \pm 37$); some of the bounce points of ScS₃ phases in their study are actually located under or near the OJP. Even though their error bars overlap, their higher values of Q_{ScS} along Fiji-MAT as compared to the rest of the west Pacific (176 versus 155) could result from a bias induced by a few of their ScS₃ phases reflecting under a high Q OJP root. This observation would generally support our results. Sipkin and Jordan's (1980) Fiji-MAT value is also in agreement with Suetsugu's (2000) ($Q_{ScS} = 172$), obtained along a similar path.

Along our reference path to CTAO, the value $Q_{ScS} = 177$ measured on the ScS₂/ScS combination is in agreement with values reported elsewhere in the western Pacific for lithosphere comparable in age (60 Ma) to the Coral Sea Basin, e.g. $Q_{ScS} = 161$ under the Philippine Sea (Revenaugh and Jordan, 1991).

In conclusion, and in contrast to the case of the CTAO paths, we fail to reproduce beneath the OJP the range of attenuation found by other investigators in neighboring provinces of the western Pacific. The

lower bounds on our value of Q_{ScS} measured under the OJP are more in line with typical values observed beneath continents, e.g. $Q_{ScS} = 285$ for continental South America (Sipkin and Jordan, 1980), in regions where the low-velocity zone is poorly, if at all, developed.

This remark is of interest, since most radial inversions of shear-wave attenuation in the mantle have shown that the latter originates mostly in the asthenosphere, and that Q_{ScS} depends primarily on the intrinsic Q_{μ} in that depth range (80–300 km), precisely where the OJP keel was inverted in Paper I. Thus, the present study, which has confirmed the slow shear velocity of the OJP root, also indicates that its material must have a high Q .

5.3. Discussion

Our results show that the root under Ontong-Java is both slower and less attenuating than typical oceanic upper mantle at comparable depths. This observation should be enough to rule out a thermal effect as the source of the root, since it has long been known and explained thermodynamically that an increase in temperature results in a decrease of both shear velocity and quality factor Q . In this section, however, we seek to quantify this statement, in view of the general uncertainty regarding intrinsic Q_{μ} values in the lower mantle. We proceed by attempting to derive from the observed deficit in velocity an estimate of Q_{ScS} expected under the assumption of a thermal anomaly. We turn our attention to comparisons with results in similarly slow provinces elsewhere and with laboratory experiments, and conclude that a thermal anomaly cannot explain our observed values of Q_{ScS} .

Only under the youngest portions of oceanic lithosphere (Evans and Sacks, 1979; Nishimura and Forsyth, 1989) or actively spreading back-arc systems have upper mantle shear velocities been found on par with our results under the OJP (locally as low as 3.9 km/s or 5% below PREM). These regions, characterized by large temperature anomalies leading to partial melting and active volcanism, are thus targets of comparison with the OJP. Little information is available, however, on the possible values of Q_{ScS} under such target regions, the mid-oceanic ridges being deprived of adequate seismic sources for multiple-ScS studies (large deep events with dip-slip

mechanisms); indeed, [Revenaugh and Jordan's \(1991\)](#) compilation of reverberated shear phases hardly samples the youngest part of the oceans ([Jordan's \(1981\)](#) tectonic regions "A"). While [Chan and Der \(1988\)](#) reported $Q_{\text{ScS}} = 138$ in the east Pacific, their study area spanned the entire Pacific basin from Tonga to South America, with reflection points sampling all lithospheric age bands; it would suggest that Q_{ScS} should be 100 or less under the East Pacific Rise (EPR). More recently, [Suetsugu \(2000\)](#) has proposed very low values, in the range 70–85, for Q_{ScS} under the South Pacific superswell, another province generally interpreted as featuring a pronounced thermal anomaly in the mantle. We conclude that in the very few cases where Q_{ScS} measurements are available for regions featuring pronounced upper mantle low-velocity anomalies, such values are significantly lower than found under the OJP.

A number of authors have used other seismic phases to report regional values of intrinsic Q_{μ} in other provinces also featuring slow wave speed anomalies. For example, under the East Pacific Rise, [Canas and Mitchell \(1978\)](#) used surface waves and [Ding and Grand \(1993\)](#) multiply reflected body-waves equivalent to surface-wave overtones, to propose $Q_{\mu} = 65$ –100 in the upper mantle. [Sheehan and Solomon \(1992\)](#) have proposed an asthenospheric Q on the order of 50 under the Mid-Atlantic Ridge using differential SS/S attenuation, but cautioned against the trade-off between the value of Q and the extent of the low- Q zone. While these studies confirmed low Q_{μ} values in the upper mantle of these provinces, the derivation of an estimate of Q_{ScS} for these regions is difficult, given the uncertainty on Q_{μ} at greater depths. The latter has been derived mostly from the attenuation of long-period surface waves and normal modes, a dataset whose scatter can reach 25%, as summarized recently by [Roult and Clévéché \(2000\)](#), and whose resolving power decreases with depth. As a result, when [Ding and Grand \(1993\)](#) combined their upper mantle Q_{μ} with available global models, even their lowest suggested estimate under the EPR, $Q_{\text{ScS}} = 173$ (using $Q_{\text{LM(RJ)}} = 231$ for the lower mantle, after [Revenaugh and Jordan \(1989\)](#)), could not be reconciled with direct measurements in a priori much older provinces (e.g. $Q_{\text{ScS}} = 141$ ([Sipkin and Jordan, 1980](#)) or $Q_{\text{ScS}} = 159$ ([Revenaugh and Jordan, 1989](#)) on the Fiji-Hawaii corridor); this discrepancy may be at-

tributable to a dependence of attenuation on frequency or to substantial lateral heterogeneity in lower mantle Q_{μ} ([Ding and Grand, 1993](#)). In this respect, and from a purely empirical point of view, for the sole purpose of extrapolating an upper mantle Q to a predicted value of Q_{ScS} an attempt to fit [Sipkin and Jordan's \(1980\)](#) dataset would suggest the use of a maximum Q_{μ} of 166 in the lower mantle; we will call this value a "modified [lower mantle] $Q_{\text{LM(mod)}}$ ", as opposed to [Revenaugh and Jordan's \(1989\)](#) $Q_{\text{LM(RJ)}} = 231$.

Another tectonic environment where large deficiencies in wave speed have been documented is the Lau Basin, behind the Tonga arc, beneath which [Van der Hilst \(1995\)](#) has used travel-time tomography to map anomalies reaching -3% . Unfortunately, we know of no direct measurement of Q_{ScS} in that province. Any such value would be difficult to interpret, since the rays would sample both the strongly attenuating back-arc structure, and the very cold, high- Q slab. However, the detailed study by [Flanagan and Wiens \(1994\)](#) has mapped areas with extreme attenuation, $Q_{\mu} = 54$ under the basin and 36 under the island arc. This result was confirmed by [Roth et al.'s \(1999\)](#) attenuation tomography, which documented Q_{μ} values of 75 under the Lau Basin. When such values ($Q_{\mu} = 36$ –54) are applied over the whole extent of the root, they translate into $Q_{\text{ScS}} = 115$ –134, using the modified lower mantle $Q_{\text{LM(mod)}}$.

In conclusion, published measurements of Q_{μ} in provinces featuring negative velocity anomalies of a magnitude comparable to that of the OJP root generally lead to estimated values of Q_{ScS} no greater than 134, and thus significantly below our observation.

Another approach consists of interpreting directly the observed anomaly in wave speed in terms of a predicted anomaly in shear attenuation. We detail here the application of three studies having addressed this problem.

- We first note the empirical relation derived by [Sipkin and Jordan \(1980\)](#) between Q_{ScS} and the two-way travel-time residuals $R_{(n+1),n}$ (in s):

$$Q_{\text{ScS}}^{-1} = 4.4 \times 10^{-4} R_{(n+1),n} + 4.88 \times 10^{-3} \quad (3)$$

These authors interpreted this correlation, obtained from data gathered in representative tectonic provinces of the earth, as favoring a thermal origin for both effects. While noting that (3) was derived

from High-Gain Long-Period datasets at similar frequencies, we use this relation with our one-way residual of 3 s ($R_{2,1} = 6$ s), to predict $Q_{\text{ScS}} = 133$, a value well outside all of our lower bounds. It is clear that the OJP dataset violates Sipkin and Jordan's (1980) relation.

- In another study, Roth et al. (2000) established a correlation between variations in P-wave speed, δV_P , and P-wave attenuation, δQ_P^{-1} , based on a tomographic study of the Tonga-Fiji area. In this framework, we will use their model to estimate a value of intrinsic attenuation in the OJP plume, based on the tomographic results of Paper I. To do so, we must first scale P- and S-wave speed anomalies according to $\delta \ln V_S / \delta \ln V_P = 1.25$ (Resovsky and Ritzwoller, 1999), which leads to an estimated $\delta V_P = -0.29$ km/s in the OJP root. We then use the empirical dataset in Roth et al. (2000) to derive a possible P-wave attenuation anomaly, by noting that their sub-dataset in the relevant depth interval (100–300 km) can be regressed as:

$$\delta Q_P^{-1} = -1.3 \times 10^{-2} \delta V_P \quad (4)$$

(δV_P is measured in km/s); we prefer this relation to their Eq. (1), which predicts a non-zero δQ_P^{-1} even for $\delta V_P = 0$, and thus cannot model the influence of temperature as the sole cause of variations in velocity and attenuation. Eq. (4) then predicts $\delta Q_P^{-1} = 0.0038$. Under the assumption of no bulk attenuation, this would in turn predict $\delta Q_\mu^{-1} = (9/4)(\delta Q_P^{-1}) \approx 0.0086$ in the root. Using model QM1, as in Roth et al. (2000), this leads to $Q_\mu = 62$ in the root, or $Q_{\text{ScS}} = 139$, using the modified $Q_{\text{LM(mod)}}$. Note that lateral heterogeneity in the OJP root would suggest that the 5% slowness anomaly is not uniform, and thus $Q_\mu = 62$ in the root is probably underestimated. A scaled down value of δV_P reflecting heterogeneity in the root would only change the final estimate of the Q_{ScS} value marginally, to $Q_{\text{ScS}} = 145$.

- Finally, we consider the experimental datasets of Sato et al. (1989a) on the variation of P-wave speed and Sato and Sacks (1989) for δQ_P^{-1} . By combining them, it is possible to infer a relationship between V_P/V_{Pm} and Q_P/Q_{Pm} , parameterized by the homologous temperature T/T_m , where the subscript m refers to the melting point of the material. In particular, these authors have shown that pressure (and

hence, depth) plays little role in the values of homologous parameters. We note that Sato et al. (1989a) interpreted shear-wave velocities of 3.9 km/s under the Iceland Plateau as 0.89 V_{Sm} , requiring $T/T_m = 1.04$ or approximately 5% in volume of melt. Under the OJP, the lithospheric velocity V_L is expected to be slightly greater than under the younger structure in Iceland (4.6 km/s as opposed to 4.5), suggesting $V_S/V_{\text{Sm}} = 0.91$, which leaves T/T_m practically unchanged, given the steep slope of homologous velocity once melting has started (see Fig. 7 of Sato et al. (1989a)). Incidentally, this result confirms that the OJP root should be partially molten if it were the result of a pure temperature anomaly. For either of the T/T_m values, Sato and Sacks' (1989) results predict $Q_P/Q_{Pm} = 0.72$ (their Fig. 1). At the pressures typical of the OJP root (5 GPa corresponding to 150 km), Sato et al.'s (1989b) Eq. (3) suggests $Q_{Pm} = 72$, which leads to $Q_P = 52$. Predicting Q_S from Q_P under conditions of partial melting may be difficult, as a finite Q_K may be involved. For a Poisson solid with infinite Q_K , we find $Q_\mu = (4/9)Q_P = 23$, while the unlikely value $Q_K = 200$, less than one-tenth of the value proposed for the asthenosphere in model WM1 (Widmer et al., 1991), leads to $Q_\mu = 27$. Note that such very low values of Q_μ have also been proposed by Canas et al. (1980) in the upper 100 km of the EPR, by Flanagan and Wiens (1990) under the active part of the Lau Basin, and by Koyanagi et al. (1995) and Talandier and Okal (1998) under Kilauea. An average value of $Q_\mu = 25$ in the root would correspond to $Q_{\text{ScS}} = 100$, using the modified $Q_{\text{LM(mod)}}$, and only 119 using Revenaugh and Jordan's (1989) lower mantle $Q_{\text{LM(RJ)}} = 231$. As explained above, the presence of lateral heterogeneity in the OJP root suggests increasing Q_P slightly in the root. However, even $Q_P = Q_{Pm} = 72$, certainly an overestimation, would lead to $Q_\mu = 32$ with $Q_K^{-1} = 0$, and then to $Q_{\text{ScS}} = 135$ using $Q_{\text{LM(RJ)}}$.

In summary, comparison with a wide range of available results on Q_{ScS} , or, at upper mantle depths, in regions featuring documented strong thermal anomalies, as well as with experimental results on peridotite, would suggest values of Q_μ in the OJP root ranging from 25 to 100, which in turn would result in Q_{ScS} under the OJP in the range 70–145, if the origin of the

structure was thermal. Despite the scatter in these estimates, due in large part to our imprecise knowledge of the bulk Earth's attenuation in the lower mantle, and under the worse case scenarios, the upper bound of the range of quality factor expected from a thermal model is $Q_{\text{ScS}} = 145$, which predicts too strong a decay of the spectral ratios with frequency, as shown by the gray lines on Fig. 7. This "thermal" Q is more than twice as small as our measured value, but more importantly, only 57% of our lower bound at 253. We reject a thermal anomaly as a possible explanation of the deficit in shear velocity in the root.

Another possible mechanism for lowering the shear-wave velocity without changing the temperature (T) would be an enhanced presence of volatiles, such as water. However, this would amount to changing the melting point T_m of the material, and hence its homologous temperature, T/T_m , which would strongly increase anelastic attenuation (Sato et al., 1989b). Indeed, the presence of minimal quantities of water is the most commonly accepted explanation for the upper mantle low-velocity zone under the oceans, which features both reduced wave speeds and high attenuation, with average values of Q_μ in the LVZ reaching below 100 (Okal and Jo, 1990). Clearly, this model cannot be applied to the case of the OJP root.

In summary, the conclusion of this study is rather unexpected, namely that the low-velocity character of the deep structure is confirmed, but that we fail to document the strong attenuation that would be expected to accompany the velocity anomaly, had its origin been thermal. This leaves a compositional (chemical) change within the major elements of the mantle silicates as the probable cause of the low-velocity root detected under the OJP. Whereas the influence of composition (such as for example, a variation in Mg number) on wave speed is now reasonably well established (e.g. Sheehan and Solomon, 1992), its effect on seismic attenuation remains at present poorly understood. Therefore, we prefer at this point, not to further speculate as to the possible chemical nature of the heterogeneity making up the OJP root.

Acknowledgements

We used GMT (Wessel and Smith, 1991) to plot figures in this paper. The reflectivity synthetics were

computed using Tim Clarke's code on which Craig Bina provided many comments. We thank Carol Stein for the compilation and discussion of the heat flow data and Michael Brown for discussion. The paper was substantially improved through the comments of Megan Flanagan, another reviewer, and Editor Ken Creager.

References

- Anderson, D.L., Theory of the Earth. Blackwell Scientific Publishers, Oxford, 1989, 366 pp.
- Bhattacharyya, J., Masters, G., Shearer, P., 1996. Global lateral variations of shear-wave attenuation in the upper mantle. *J. Geophys. Res.* 101, 22273–22289.
- Bott, M.H.P., Gunnarsson, K., 1980. Crustal structure of the Iceland-Færø Ridge. *J. Geophys.* 47, 221–227.
- Canas, J.A., Mitchell, B.J., 1978. Lateral variation of surface-wave attenuation across the Pacific. *Bull. Seismol. Soc. Am.* 68, 1637–1650.
- Canas, J.A., Mitchell, B.J., Correig, A.M., 1980. Q_β^{-1} models for the East Pacific Rise and Nazca plate. In: Davies, P.A., Runcorn, S.K. (Ed.), *Mechanisms of Plate Tectonics and Continental Drift*. Academic Press, San Diego, pp. 123–133.
- Chan, W.W., Der, Z., 1988. Attenuation of multiple ScS in various parts of the world. *Geophys. J.* 92, 303–314.
- Ding, X.-Y., Grand, S.P., 1993. Upper mantle Q structure beneath the East Pacific Rise. *J. Geophys. Res.* 98, 1973–1985.
- Dziewonski, A.M., Anderson, D.L., 1981. Preliminary reference Earth model. *Phys. Earth Planet Inter.* 25, 297–356.
- Dziewonski, A.M., Gilbert, F., 1976. The effect of small, aspherical perturbations on travel times and a re-examination of the corrections for ellipticity. *Geophys. J. R. Astronom. Soc.* 44, 7–17.
- Dziewonski, A.M., Ekström, G., Salganik, M.P., 1997. Centroid-moment tensor solutions for April–June 1996. *Phys. Earth Planet. Inter.* 102, 11–20.
- Efron, B., 1982. *The Jackknife, the Bootstrap and Other Resampling Plans*. Society for Industrial and Applied Mathematics, Bristol, 92 pp.
- Evans, J.R., Sacks, I.S., 1979. Deep structure of the Iceland Plateau. *J. Geophys. Res.* 84, 6859–6866.
- Flanagan, M.P., Wiens, D.A., 1990. Attenuation structure beneath the Lau back-arc spreading center from teleseismic S phases. *Geophys. Res. Lett.* 17, 2117–2120.
- Flanagan, M.P., Wiens, D.A., 1994. Radial upper mantle attenuation structure of inactive back-arc basins from differential shear-wave measurements. *J. Geophys. Res.* 99, 15469–15485.
- Jordan, T.H., 1981. Global tectonic regionalization for seismological data analysis. *Bull. Seismol. Soc. Am.* 71, 1131–1141.
- Kanamori, H., 1967. Spectrum of short-period core phases in relation to the attenuation in the mantle. *J. Geophys. Res.* 72, 2181–2186.
- Klosko, E.R., Russo, R.M., Okal, E.A., Richardson, W.P., 2001. Evidence for a rheologically strong chemical mantle root beneath the Ontong-Java Plateau. *Earth Planet. Sci. Lett.* 186, 347–361.

- Kovach, R.L., Anderson, D.L., 1964. Attenuation of shear waves in the upper and lower mantle. *Bull. Seismol. Soc. Am.* 54, 1855–1864.
- Koyanagi, S., Aki, K., Biswas, N., Mayeda, K., 1995. Inferred attenuation from the effect-corrected T phases recorded on the Island of Hawaii. *Pure Appl. Geophys.* 144, 1–17.
- Lees, J.M., Lindley, G.T., 1994. Three-dimensional attenuation tomography at Loma Prieta: inversion of t^* for Q . *J. Geophys. Res.* 99, 6843–6863.
- Mahoney, J.J., Storey, M., Duncan, R.A., Spencer, K.J., Pringle, M., 1993. Geochemistry and geochronology of the Ontong-Java Plateau. In: Pringle, M., Sager, W., Sliter, W., Stein, S. (Eds.), *The Mesozoic Pacific: Geology, Tectonics, and Volcanism*, Am. Geophys. Un. Geophys. Monogr. 77, 233–261.
- Nishimura, C.L., Forsyth, D.W., 1989. The anisotropic structure of the upper mantle in the Pacific. *Geophys. J. Int.* 96, 203–229.
- Okal, E.A., Anderson, D.L., 1975. A study of lateral inhomogeneities in the upper mantle by multiple ScS travel-time residuals. *Geophys. Res. Lett.* 2, 313–316.
- Okal, E.A., Jo, B.G., 1990. Q measurements for phase X overtones. *Pure Appl. Geophys.* 132, 331–362.
- Papoulis, A., 1973. Minimum bias windows for high resolution spectral estimates. *IEEE Trans. Inform. Theory* 19, 9–12.
- Resovsky, J.S., Ritzwoller, M.H., 1999. Regularization uncertainty in density models estimated from normal mode data. *Geophys. Res. Lett.* 26, 2319–2322.
- Revenaugh, J., Jordan, T.H., 1989. A study of mantle layering beneath the western Pacific. *J. Geophys. Res.* 94, 5787–5813.
- Revenaugh, J., Jordan, T.H., 1991. Mantle layering from ScS reverberations. 1. Waveform inversion of zeroth-order reverberations. *J. Geophys. Res.* 96, 19749–19762.
- Richardson, W.P., Okal, E.A., Van der Lee, S., 2000. Rayleigh-Wave Tomography of the Ontong-Java Plateau. *Phys. Earth Planet Inter.* 118, 29–51.
- Riedel, K.S., Sidorenko, A., 1995. Minimum bias multiple taper spectral estimation. *IEEE Trans. Signal Proc.* 43, 188–195.
- Roth, E.G., Wiens, D.A., Dorman, L.M., Hildebrand, J., Webb, S.C., 1999. Seismic attenuation tomography of the Tonga-Fiji region using phase pair methods. *J. Geophys. Res.* 104, 4795–4809.
- Roth, G.R., Wiens, D.A., Zhao, D., 2000. An empirical relationship between seismic attenuation and velocity anomalies in the upper mantle. *Geophys. Res. Lett.* 27, 601–604.
- Roult, G., Clévéché, E., 2000. New refinements in attenuation measurements from free-oscillation and surface-wave observations. *Phys. Earth Planet. Inter.* 121, 1–37.
- Sato, H., Sacks, I.S., 1989. Anelasticity and thermal structure of the oceanic upper mantle: temperature calibration with heat flow data. *J. Geophys. Res.* 94, 5705–5715.
- Sato, H., Sacks, I.S., Murase, T., 1989a. The use of laboratory velocity data for estimating temperature and partial melt fraction in the low-velocity zone: comparison with heat flow and electrical conductivity studies. *J. Geophys. Res.* 94, 5689–5704.
- Sato, H., Sacks, S., Murase, T., Muncill, G., Fukuyama, H., 1989b. Q_P melting temperature relation in peridotite at high pressure and temperature: attenuation mechanism and implications for the mechanical properties of the upper mantle. *J. Geophys. Res.* 94, 10647–10661.
- Sheehan, A.F., Solomon, S.C., 1992. Differential shear-wave attenuation and its lateral variation in the North Atlantic region. *J. Geophys. Res.* 97, 15339–15350.
- Sipkin, S.A., Jordan, T.H., 1976. Lateral heterogeneity of the upper mantle determined from the travel times of multiple ScS. *J. Geophys. Res.* 81, 6307–6320.
- Sipkin, S.A., Jordan, T.H., 1980. Regional variation of Q_{ScS} . *Bull. Seismol. Soc. Am.* 70, 1071–1102.
- Slepian, D., 1978. Prolate spheroidal wave functions, Fourier analysis and uncertainty. V. The discrete case. *Bell Syst. Technol. J.* 5, 1371–1429.
- Suetsugu, D., 2000. Average velocity and attenuation in the mantle beneath the south Pacific from multiple ScS waves. *Eos. Trans. Am. Geophys.* 81 (22), WP198 (Abstract).
- Talandier, J., Okal, E.A., 1987. Crustal structure in the society and Tuamotu Islands, French Polynesia. *Geophys. J.R. Astronom. Soc.* 88, 499–528.
- Talandier, J., Okal, E.A., 1998. On the mechanism of conversion of seismic waves to and from T waves in the vicinity of island shores. *Bull. Seismol. Soc. Am.* 88, 621–632.
- Thomson, D.J., 1982. Spectrum estimation and harmonic analysis. *Proc. IEEE* 70, 1055–1096.
- Thomson, D.J., Chave, A., 1991. Jackknifed error estimates for spectra, coherence, and transfer functions. In: Haykin, S. (Ed.), *Advances in Spectrum Analysis and Array Processing*, vol. 1, Prentice-Hall, Englewood Cliffs.
- Van der Hilst, R.D., 1995. Complex morphology of subducted lithosphere in the mantle beneath the Tonga trench. *Nature* 374, 154–157.
- Wessel, P., Smith, W.H.F., 1991. New version of generic mapping tools released. *Eos. Trans. AGU* 72, 445–446.
- Widmer, R., Masters, G., Freeman, G., 1991. Spherically symmetric attenuation within the Earth from normal mode data. *Geophys. J. Int.* 104, 541–553.
- Woods, M.T., Okal, E.A., 1994. The structure of the Nazca Ridge and Sala y Gomez Seamount Chain from the dispersion of Rayleigh waves. *Geophys. J. Int.* 117, 205–222.
- Woods, M.T., Okal, E.A., 1996. Rayleigh-wave dispersion along the Hawaiian Swell: a test of lithospheric thinning by the thermal rejuvenation at a hotspot. *Geophys. J. Int.* 125, 325–339.
- Yoshida, Y., Suetsugu, D., 2000. Lithospheric structure in French Polynesia region using Rayleigh wave phase velocity. *Eos. Trans. Am. Geophys.* 81 (22), WP198 (Abstract).
- Yoshida, M., Tsujiura, M., 1975. Spectrum and attenuation of multiply reflected core phases. *J. Phys. Earth* 23, 31–42.